PROTEINS: Structure, Function, and Bioinformatics 55:805–813 (2004)

Ultrahigh Resolution Drug Design. II. Atomic Resolution Structures of Human Aldose Reductase Holoenzyme Complexed with Fidarestat and Minalrestat: Implications for the Binding of Cyclic Imide Inhibitors

Ossama El-Kabbani,[1] Connie Darmanin,[1] Thomas R. Schneider,[2] Isabelle Hazemann,[3] Federico Ruiz,[3] Mitsuru Oka,[4] Andrzejj Joachimiak,[5] Clemens Schulze-Briese,[6] Takashi Tomizaki,[6] Andre Mitschler,[3] and Alberto Podjarny[3]*

[1]*Department of Medicinal Chemistry, Victorian College of Pharmacy, Monash University (Parkville Campus), Parkville, Victoria, Australia*
[2]*Department of Structural Chemistry, University of Götingen, Göttingen, Germany*
[3]*UPR de Biologie Structurale, IGBMC, CNRS INSERM ULP, Illkirch, France*
[4]*Sanwa Kagaku Kenkyusyo Company, Ltd., Mie, Japan*
[5]*Structural Biology Center, Argonne, Illinois*
[6]*Swiss Light Source at PSI, Villigen, Switzerland*

ABSTRACT **The X-ray structures of human aldose reductase holoenzyme in complex with the inhibitors Fidarestat (SNK-860) and Minalrestat (WAY-509) were determined at atomic resolutions of 0.92 Å and 1.1 Å, respectively. The hydantoin and succinimide moieties of the inhibitors interacted with the conserved anion-binding site located between the nicotinamide ring of the coenzyme and active site residues Tyr48, His110, and Trp111. Minalrestat's hydrophobic isoquinoline ring was bound in an adjacent pocket lined by residues Trp20, Phe122, and Trp219, with the bromo-fluorobenzyl group inside the "specificity" pocket. The interactions between Minalrestat's bromo-fluorobenzyl group and the enzyme include the stacking against the side-chain of Trp111 as well as hydrogen bonding distances with residues Leu300 and Thr113. The carbamoyl group in Fidarestat formed a hydrogen bond with the main-chain nitrogen atom of Leu300. The atomic resolution refinement allowed the positioning of hydrogen atoms and accurate determination of bond lengths of the inhibitors, coenzyme $NADP^+$ and active-site residue His110. The 1′-position nitrogen atom in the hydantoin and succinimide moieties of Fidarestat and Minalrestat, respectively, form a hydrogen bond with the Nϵ2 atom of His 110. For Fidarestat, the electron density indicated two possible positions for the H-atom in this bond. Furthermore, both native and anomalous difference maps indicated the replacement of a water molecule linked to His110 by a Cl-ion. These observations suggest a mechanism in which Fidarestat is bound protonated and becomes negatively charged by donating the proton to His110, which may have important implications on drug design. Proteins 2004;55:805–813.**

Key words: aldose reductase; atomic resolution; X-ray crystallography; ternary complex; inhibitor binding

INTRODUCTION

Aldose reductase (ALR2; EC 1.1.1.21), a member of the aldo-keto reductase superfamily, is a 36-kDa enzyme that catalyzes the NADPH-dependent reduction of diverse aldehydes to their corresponding alcohols.[1,2] ALR2, the first and rate-determining enzyme of the polyol pathway, converts glucose to sorbitol, which is subsequently transformed to fructose by sorbitol dehydrogenase. Although no physiological role has been established for ALR2, the accumulation of excess sorbitol resulting from diabetic hyperglycemia plays a role in the development of diabetic complications such as retinopathy, neuropathy, and nephropathy.[3,4] Thus, inhibition of ALR2 offers a potential treatment for the debilitating pathologies associated with chronic hyperglycemia that occurs with diabetes mellitus.[5,6] Many aldose reductase inhibitors (ARIs) have been reported in the literature; however, because of unacceptable side effects and lack of efficacy, most drug candidates were not approved for clinical use. Nevertheless, ARIs are commercially available in some countries, and several new potential candidates are currently undergoing clinical trials.[6,7]

Abbreviations: ALR1, aldehyde reductase; ALR2, aldose reductase; ARI, aldose reductase inhibitor; $NADP^+$, nicotinamide adenine dinucleotide phosphate.

Grant sponsor: Australian Research Council; Grant sponsor: Monash University Research Fund; Grant sponsor: Sanwa Kagaku Kenkyusyo Company, Ltd.; Grant sponsor: Centre Natioanl de la Recherche Scientifique (CNRS); Grant sponsor: collaboration CERC-CNRS; Grant sponsor: Ecos Sud; Grant sponsor: Institut National de la Santé et de la Recherche Médicale (INSERM); Grant sponsor: Hôopital Universitare de Strasbourg (HUS).

*Correspondence to: Alberto Podjarny, UPR de Biologie Structurale, IGBMC, CNRS INSERM ULP, 1 rue Laurent Fries, B.P. 163, 67404 Illkirch, France. E-mail: podjarny@igbmc.u-strasbg.fr

Received 18 May 2003; Accepted 21 September 2003

Published online 27 February 2004 in Wiley InterScience (www.interscience.wiley.com). DOI: 10.1002/prot.20001

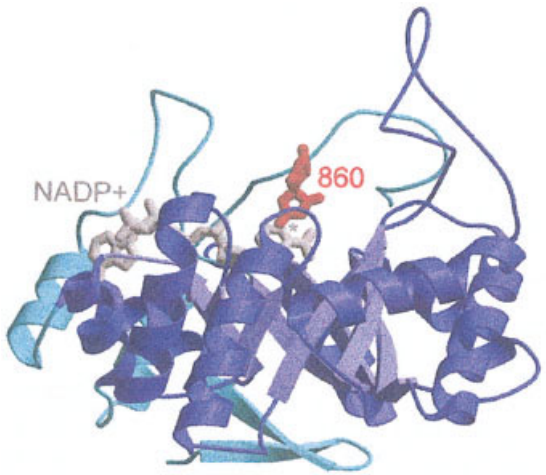

Fig. 1. Overall ribbon view of the ALR2 ternary structure. The TIM barrel is shown with the axis vertical, helices in blue, and sheets in dark gray. Extra sheets and helices are shown in cyan, $NADP^+$ is shown in light gray and Fidarestat is shown in red. Note that $NADP^+$ sits on top of the TIM barrel, and Fidarestat is surrounded by loops protruding from the barrel. The nicotinamide ring, which defines the active site, is marked by an *.

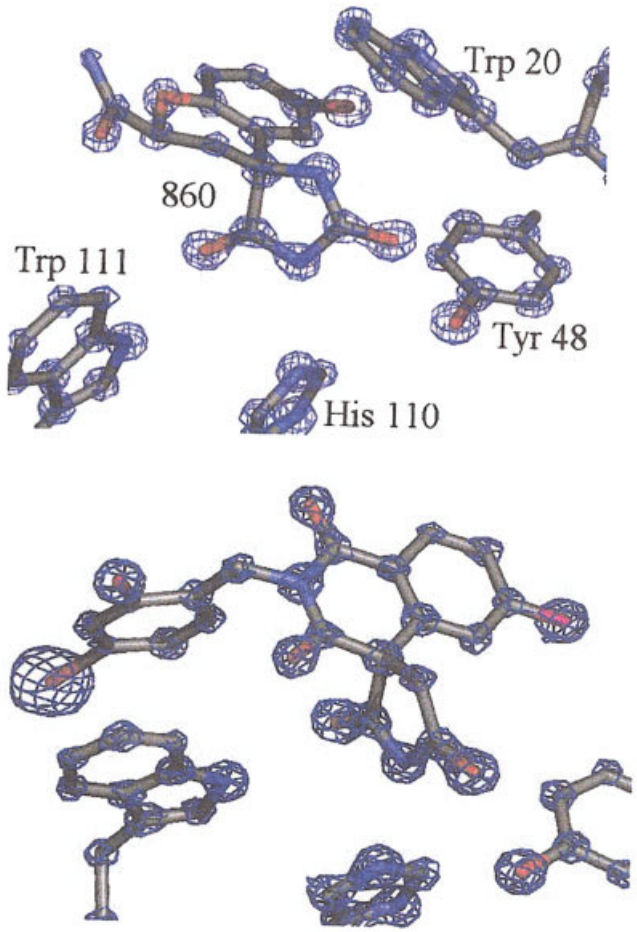

Fig. 2. SigmaA-weighted $2F_oF_c$ maps calculated with a 4.0 σ cutoff superimposed on the final models of the active site with (**a**) Fidarestat (860) bound and (**b**) Minalrestat (509) bound.

Inhibitors of ALR2 characteristically have a polar group attached to a hydrophobic ring system.[8] The two main categories of ALR2 inhibitors are those having a cyclic imide moiety represented by a hydantoin (imidazoline-2,4-dione), succinimide, or a related ring system and those containing an acetic acid moiety. Although the activities of the cyclic imide and carboxylic acid derivatives are similar *in vitro*, cyclic imide derivatives are usually more potent *in vivo*, likely because of differences in their pharmacokinetic properties, such as pKa values. The pKa for a drug is an important parameter to consider because the ionization of the drug at physiological pH would make it difficult to cross the biological membrane. The substitution of an acetic acid group with a cyclic imide derivative was shown to transform compounds active as ARIs almost exclusively *in vitro* to compounds with *in vivo* potency.[9–11] Although there are only a few cyclic imide derivative compounds in clinical trials, the encouraging results obtained by Fidarestat were reported recently. The results showed that Fidarestat inhibited structural and functional progressions of diabetic neuropathy[12] and halted the increase in sorbitol pathway flux in patients with diabetes.[13]

Crystal structures of ALR2-inhibitor complexes (see Fig. 1 for an overview) have shown that the polar hydantoin and carboxylate groups bind in an anion-binding site between the nicotinamide ring of the coenzyme and ALR2 residues Tyr48, His110, and Trp111.[14–18] Hydrogen bonds are formed between these three active-site residues and the polar group of the inhibitor. The hydrophobic ring systems of the inhibitors are bound tightly in a pocket that is adjacent to the anion-binding site. Moreover, biochemical and crystallographic studies have shown that inhibitors specific to ALR2 interact with C-terminal residues that are not conserved in the homologous aldehyde reductase (ALR1)[19,20] by binding to a subsite, which has been described as the "specificity" pocket.[14–18,21–24] The activities of ARIs against ALR1, a member of the aldo-keto reductase superfamily that is closely related to ALR2 (65% identity), are usually assessed to test inhibitor selectivity for ALR2.

Here we present the first atomic resolution structures of human aldose reductase holoenzyme in complex with cyclic imide inhibitors and provide experimental evidence for the negatively charged 1′-position nitrogen atom of the cyclic imide derivative bound in the active site of the enzyme. The crystal structures were determined for the complexes with the bound inhibitors Fidarestat ((2*S*,4*S*)-6-Fluoro-2′,5′-dioxospiro[chroman-4,4′-imidazoline]-2-carboxamide) and Minalrestat (2[4-bromo-2-fluorophenyl)-methyl]-6-fluorospiro[isoquinoline-4-(1*H*),3′-pyrrolidine]-1,2′,3,5′(2*H*)-tetrone) (Scheme 1) at resolutions of 0.92 Å and 1.1 Å, respectively. The atomic resolution structures allowed the determination of multiple conformations for several amino acid side-chains and H-atom positions in the active-site region. For Fidarestat, they also showed the presence of a Cl- atom near His110. This information was used to identify the protonation states of the bound inhibitors and the active site residues. The imidazole side-chain of the catalytic His110 forms a hydrogen bond

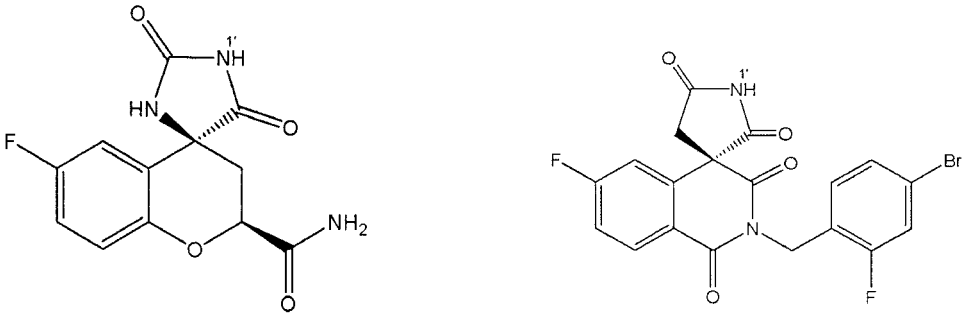

Scheme 1.

with the 1′-position nitrogen atom of the hydantoin and succinimide rings. The negatively charged heads of the inhibitors are bound tightly in the anion-binding pocket with the halogenated benzyl substituent of Minalrestat and the carbamoyl group of Fidarestat entering the specificity pocket.

MATERIALS AND METHODS

Expression and Purification of Human ALR2

The open reading frame of the human ALR2 gene (Accession Gene Bank/EMBL Data Bank Number J05017) was amplified by polymerase chain reaction (PCR) from complementary deoxyribonucleic acid (cDNA)[25] and cloned into the T7 RNA polymerase-based vector pET15b (Novagen). Expression of the hexahistidine tagged protein in the *E. coli* strain BL21 (DE3) (Novagen) was induced by IPTG (Euromedex) during a 3-h period at 37°C. The pellet from a 4-L culture was disrupted by sonication and centrifuged. The supernatant was loaded onto a Talon metal-affinity column (Clontech). After thrombin cleavage of the hexahistidine extension, the detagged protein was loaded onto a DEAE Sephadex A-50 column (Pharmacia) and eluted with a NaCl gradient.[26]

Crystallization

Before crystallization, human ALR2 at 16 mg/mL in 50 mM ammonium citrate buffer (pH 5) was mixed with the oxidized form of nicotinamide-adenine-dinucleotide phosphate ($NADP^+$) and inhibitor (molar ratio of ALR2:$NADP^+$:inhibitor was 1:2:2.5). The ternary complexes were crystallized by using the vapor diffusion method. The ALR2/$NADP^+$/inhibitor solution was mixed with an equal volume of 15% (w/v) polyethylene glycol (PEG) 6000 in 50 mM ammonium citrate buffer (pH 5), and 10-μL hanging droplets were placed above a well solution (1 mL) containing 20% PEG 6000 and 120 mM ammonium citrate. Crystals were grown at 277 K, transferred into a stabilization solution (25% PEG 6000), then into cryoprotecting solution (40% PEG 6000), and dipped into liquid nitrogen.

X-Ray Data Collection and Processing

The holoenzyme complexed with Fidarestat and Minalrestat crystallized in monoclinic $P2_1$ and triclinic *P1* space groups, respectively, with unit cell parameters a = 49.43 Å, b = 67.04 Å, c = 47.32 Å and β = 92.1° (at 100 K), and a = 40.02 Å, b = 47.13 Å, c = 47.37 Å, α = 75.7°, β = 67.5°, and γ = 76.8° (at 100 K), respectively. There was one monomer per asymmetric unit, consisting of 316 amino acid residues. The solvent content was estimated to occupy 34.6% and 34.8% of the unit cell volume,[27] respectively. Near completion, synchrotron data sets were collected at the Swiss Light Source beamline X06SA and Advanced Photon Source beamline BM19 from one Fidarestat and one Minalrestat complexed crystals, respectively, and processed using the programs *HKL2000* and SCALEPACK.[28] The exposure time (1–15 s), oscillation range (0.2–1°), detector geometry (2θ 0–30°), and crystal-detector distance (130–200 mm) were adjusted to optimize each data set. Crystals proved resistance to radiation damage at 100 K, allowing the measurements of 2 × 180° zones in reciprocal space for near complete data sets between low- and high-resolution ranges. Data collection and processing statistics are shown in Table I.

Structure Refinement

The coordinates of human ALR2[29] were used to solve the structure by molecular replacement.[30] Crystallographic refinement involved repeated cycles of conjugate gradient energy minimization, simulated annealing, and temperature factor refinement.[30] Refinement statistics are presented in Table I. Amino acid side-chains were fitted into $2F_o$-F_c and F_o-F_c electron density maps. The final $2F_o$-F_c maps (Fig. 2) showed clearly the atomic electron density for Fidarestat and Minalrestat. The F_o-F_c electron density maps for Fidarestat showed a strong peak located at the position of the water molecule near His110. Very clear anomalous difference maps, phased with the model, showed a strong peak in this position [Fig. 3(a)], which indicated the atom to be a Cl, a P, or an S. The environment corresponds to a Cl^- ion [Fig. 3(b)]. However, when a full occupancy of a Cl^- ion was introduced, a strong negative peak (−7 σ) appeared in the difference map. This was interpreted as evidence that the site was occupied simultaneously, partially by a Cl^- ion and partially by a water molecule. The water position, estimated from the Minalrestat structure, is ~0.1 Å closer to the protein than the Cl^- position clearly indicated by the anomalous peak. Because this small difference in positions cannot be reliably refined independently, the water O and the Cl^- atoms in the

TABLE I. Data Collection and Refinement Statistics

	Fidarestat	Minalrestat
Data collection and processing		
No. of crystals used	1	1
Wavelength (Å)	0.90042	0.97934
Space group	$P2_1$	$P1$
Unit cell parameters		
a, b, c (Å)	49.4, 67.0, 47.3	40.0, 47.1, 47.4
α, β, γ (°)	90.0, 92.1, 90.0	75.7, 67.5, 76.8
Diffraction data		
Resolution range (Å)	99.0–0.92	50.0–1.1
Unique reflections	193488	115145
$R(I)_{merg}$ (overall) (%)	3.6	4.10
$R(I)_{merg}$ ([a]) (%)	15.90	9.21
Completeness (overall) (%)	91.90	92.60
Completeness ([a]) (%)	83.70	81.50
Redundancy (overall)	3.20	3.63
Redundancy ([a])	2.96	3.13
I/σ(I) (overall)	13.45	25.60
I/σ (I) ([a])	5.37	11.75
Refinement		
Resolution range (Å)	10–0.92	10–1.1
Reflections used in refinement (work/test)	183647/9675	108743/6391
R values for all reflections (work/test)		
Isotropic refinement		
R_{cryst}/R_{free} without H (%)	18.4/21.0	16.7/18.9
Anisotropic refinement		
R_{cryst}/R_{free} with H (%)	10.4/12.8	9.9/12.4
R_{cryst}/R_{free} without H (%)	11.6/14.3	11.0/13.7
Reflections with $F > 4\sigma_F$ (work/test)	158527/8343	103774/5461
R values based on $F > 4\sigma_F$		
Isotropic refinement		
R_{cryst}/R_{free} without H (%)	12.0/14.9	16.4/18.5
Anisotropic refinement		
R_{cryst}/R_{free} with H (%)	9.9/12.2	9.5/12.1
R_{cryst}/R_{free} without H (%)	11.1/13.7	10.7/13.3
Protein residues	316	316
Coenzyme	1	1
Inhibitor	1	1
Water molecules	597	427
RMSDs		
Bonds (Å)	0.012	0.013
Angles (°)	1.95	1.75
Dihedrals (°)	8.87	8.55
Ramachandran plot		
Residues in most favored regions (%)	91.0	90.6
Residues in additional allowed regions (%)	9.0	9.4
Estimated coordinate error		
Luzzati mean error[44] (Å)	0.044	0.035
Mean B factor (Å^2)		
Protein	13.7	13.4
$NADP^+$	7.95	6.47
Inhibitor	7.22	6.87

[a]Data in the highest resolution shell are given in parentheses for Fidarestat and Minalrestat between 0.96 and 0.92 Å and 1.16 and 1.1 Å, respectively.

Fidarestat structure were assumed to be superimposable. To determine the Cl^- occupancy, a systematic series of refinements was done: the position of both Cl^- and water were fixed to one single position, and their B-values were constrained to be identical, whereas the occupancies were varied from 0 to 1 at steps of 0.1 (see Table II), and the difference map was inspected in each run. The smallest signal in the difference map ($<1\ \sigma$) was obtained for occupancies of 0.6 for Cl^- and 0.4 for water. For this combination of occupancies, the common B-value for the Cl^- and the water site refined to a value of 6.0 Å^2. This refined value is similar to the ones for the atoms surrounding the site and thus supports the model with two partially occupied atomic species in one position. There was no evidence for the Cl^- ion in the Minalrestat

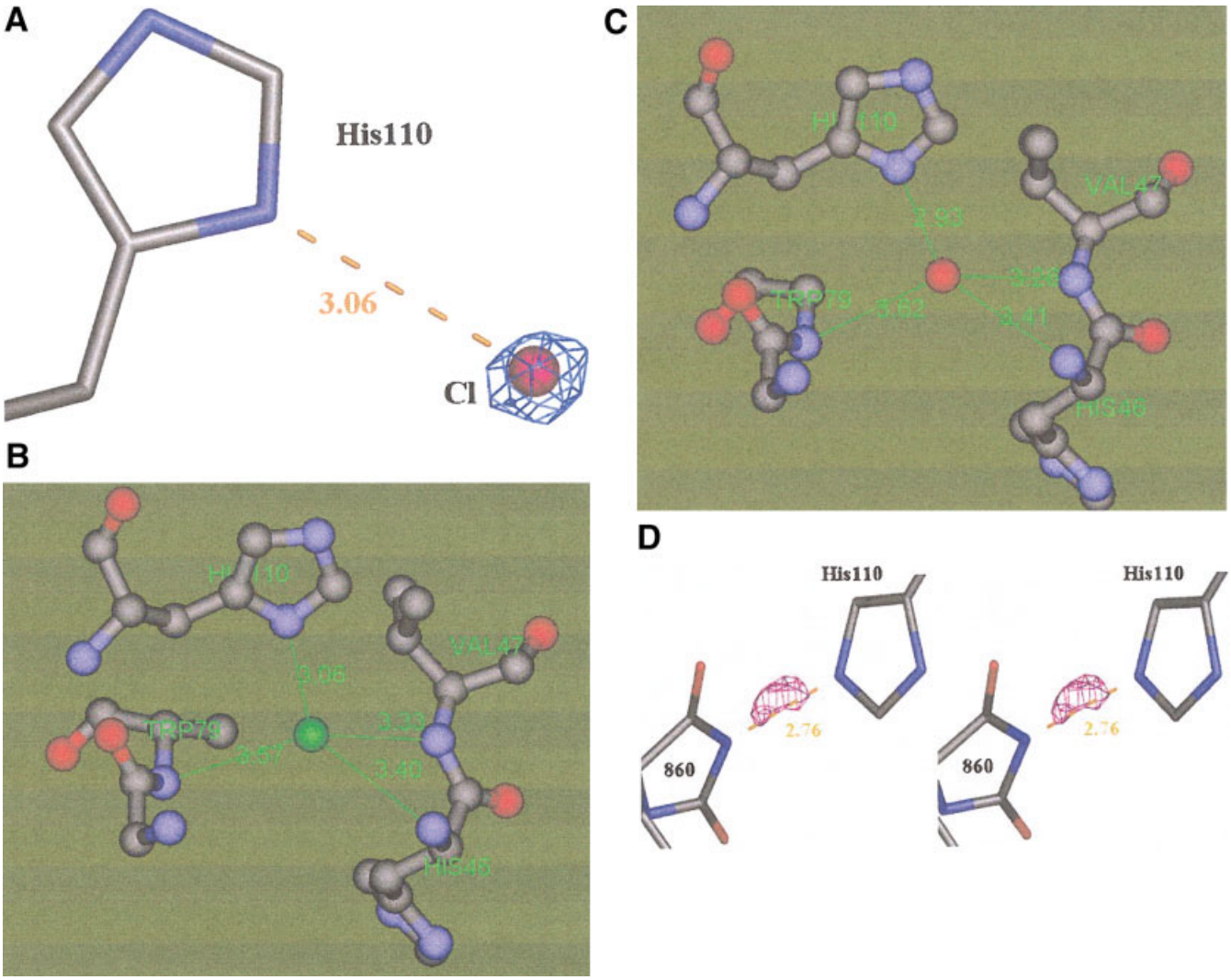

Fig. 3. Anomalous difference map (**a**) showing the peak corresponding to the Cl^- ion (**b**) environment of the Cl^- ion in Fidarestat. Similar distances to N-atoms are observed in Haloalkane Dehalogenase[45] (**c**) environment of the water molecule near His110 in Minalrestat (**d**) SigmaA-weighted F_oF_c map of the active-site region with omitted hydrogens calculated with a 2.5 σ cutoff superimposed on the final model of the active site with Fidarestat (860) bound. The elongated peak corresponds to the protonation of His110 at Nε2 and to the protonation of Fidarestat in the 1′-position N atom.

TABLE II. Results of Different Refinement Runs

occ(Cl-) [fract]	B(Cl-,O)[Å^2]	Diff.Dens (Cl-) [σ(Fo-Fc)]
0.0	2.08	+11
0.1	2.95	+9
0.2	3.70	+7
0.3	4.36	+5
0.4	4.95	+2.5
0.5	5.49	<2
0.6	5.99	<1
0.7	6.45	−3
0.8	6.89	−5
0.9	7.30	−6
1.0	7.69	−7

Occ(Cl-) is the value to which occupancy of Cl- was fixed; water O has an occupancy of 1.0-Occ(Cl-). B(Cl-,O) is the B-value of both Cl- and O after 20 cycles of conjugate gradient least-squares refinement (note that the two values were constrained to be identical). Diff.Dens (Cl-) is Fo-Fc difference density measured at the position of Cl-/O.

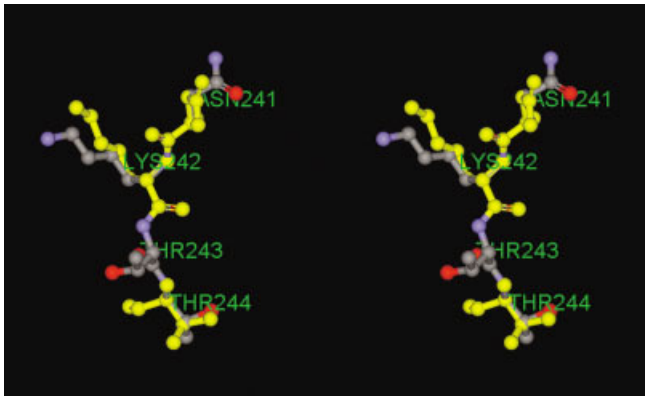

Fig. 4. Stereoview for the region Asn241-Lys242-Thr243-Thr244 in the ALR2 holoenzyme in complex with Minalrestat showing the double conformations for the side-chains of Lys242 and Thr244.

maps, and the geometry of the site corresponds to a water molecule and not to a Cl^-ion [Fig. 3(c)]. Water molecules were located in a difference map, and anisotropic conjugate gradient refinement was conducted by using the *SHELX* program package.[31] In the final cycles, riding H-atoms were introduced, including observed protonation states for the inhibitor and His110. The programs *TURBO*-FRODO[32] and *XtalView*/Xfit[33] were used for fitting the models into the electron density. The difference electron density maps allowed the identification of the protonation states of the inhibitors and active-site residue His110 [Fig. 3(d)] and multiple conformations for several amino acid residue sidechains (Fig. 4).

RESULTS AND DISCUSSION

X-Ray Crystallography

The structures of the holoenzyme in complex with Fidarestat and Minalrestat were determined at 0.92 Å resolution and 1.1 Å resolution, respectively, with final R_{cryst} of 9.9% and 9.5% and R_{free} of 12.2% and 12.1%, respectively (Table I). The asymmetric unit consisted of 316 amino acids, 1 $NADP^+$ coenzyme, 1 inhibitor, and solvent molecules (597 and 427, respectively), and a Cl^- ion for Fidarestat. A ϕ, ψ plot of main-chain torsion angles placed 91% and 9% of the ALR2 residues in the most favored and additional allowed regions, respectively.[34,35] The statistics for stereochemistry and geometry of the final models are shown in Table I.

Stereo diagrams of the inhibitors bound to the active site of ALR2 are presented in Figure 5. The overall structure of human ALR2 folds into an eight-strand α/β-barrel with the active site located on the C-terminal end of the barrel.[36] The $NADP^+$-binding site is located adjacent to a hydrophobic active-site pocket. As previously observed in crystal structures of ALR2 in complex with hydantoin inhibitors,[15,18] Fidarestat and Minalrestat are bound in the active site with their hydantoin and succinimide moieties entering the anion-binding site. These moieties are held in place by 13 van der Waals interactions with the nicotinamide ring of $NADP^+$. Thus, the inhibitors' polar heads are firmly anchored in the active site, contributing to the high quality of the electron densities observed for the Fidarestat and Minalrestat molecules (Fig. 2). Both carbonyl oxygen atoms are present within hydrogen bonding distances from the Nϵ1 atom of Trp111 (2.80 Å and 2.87 Å, respectively) and the OH group of Tyr48 (2.63 Å and 2.60 Å, respectively). His110 forms a hydrogen bond with the 1′-position nitrogen atom in the cyclic imide substituents of Fidarestat and Minalrestat (2.76 Å and 2.80 Å, respectively). Peaks in the electron density clearly indicate two positions for the H-atom in this bond for Fidarestat. For Minalrestat, only one peak is seen near His110-Nϵ2, as proposed in Figure 6, scheme 2. Furthermore, the C—O bond distances in the cyclic imide rings are within 0.04 Å of a double bond, excluding the protonation of the oxygen atoms. These observations led to the conclusion that the inhibitors can have different protonation states, which may have important implications on the design of cyclic imide inhibitors (Figs. 2, 3 and 5). In Fidarestat, the presence of the Cl^- ion strongly suggests that the inhibitor is bound neutral and that the Cl^- ion is incorporated to compensate the charge of $NADP^+$, which in the native crystal state is compensated by a citrate ion. Figure 6 shows a scheme of the possible binding mechanisms.

Although cyclic imide and carboxylic acid ARIs have comparable activities *in vitro*, the exchange of the acetic acid functional group with a cyclic imide substituent has been found to transform the compound from being exclusively active *in vitro* to a compound with high potency in vivo,[9–11] likely due to accompanied changes in the pharmacokinetic properties of the compound, such as the pKa value. Carboxylic acids have low pKa values (generally $<$ 4) that make them ionized at physiological pH and more difficult to cross the biological membrane than cyclic imides, which have higher pKa values (between 8 and 9).[37] It is of interest that the experimentally measured pKa value (pKa = 8.2) for the catalytic residue Tyr48 has been shown to be ~2.5 units lower than the pKa value calculated for a Tyr residue in solution.[38] Similarly, the presence of the cyclic imide substituents of Fidarestat and Minalrestat in close proximity with the positively charged nicotinamide ring of the coenzyme and the protonated Nϵ2 of His110 could lower the pKa value of the cyclic imide substituent, resulting in a partial population of inhibitors, which would be negatively charged at the 1′-position nitrogen atom at the crystallization pH of 5.0. Biochemical and crystallographic studies have suggested that ARIs preferably bind to the ALR2/$NADP^+$ complex, whereas the substrates bind to the ALR2/NADPH form.[15,39] At the physiological pH, the inhibitor population that is negatively charged at the 1′-position nitrogen atom in the cyclic imide substituent would interact favorably with the protonated Nϵ2 atom of His110 and positively charged nicotinamide of the coenzyme. The inhibitor population, which is neutral, could also bind in the active site, provided that another negatively charged moiety, such as the Cl^- ion observed in the anomalous maps of Fidarestat, would bind simultaneously to compensate the charge of the displaced citrate, originally bound in the native site. The simultaneous presence of different positions of the H-atom in the N1Nϵ2 hydrogen bond and of two different ligands (water and Cl^-) bound to His110 suggests different modes of binding, as schematized in Figure 6. This scheme shows the following states:

1a). In the native configuration, the active site is occupied by a citrate ion (observed in the native structure) that compensates the charge of $NADP^+$.

1b). Part of the inhibitor binds in neutral state, displacing the citrate ion. Simultaneously, a Cl^- ion replaces the water molecule. This happens for Fidarestat in ~60% of the cases (as indicated by the Cl^- occupation) and does not happen in Minalrestat.

1c). In Fidarestat, the presence of the Cl^- ion shifts positively the pKa of His110, as indicated by theoretical calculations (Ruiz et al., article in preparation). The histidine accepts the proton from the N1 atom of the hydantoin. An electrostatic interaction appears

between the charged histidine and the charged inhibitor.

2. Alternatively, a charged population of the inhibitor is bound in a way similar to that observed for the carboxylic acid inhibitors. In Fidarestat, the occupation of the water molecule bound to His110 suggests that this happens in ~40% of the cases. In Minalrestat, this happens for all the cases.

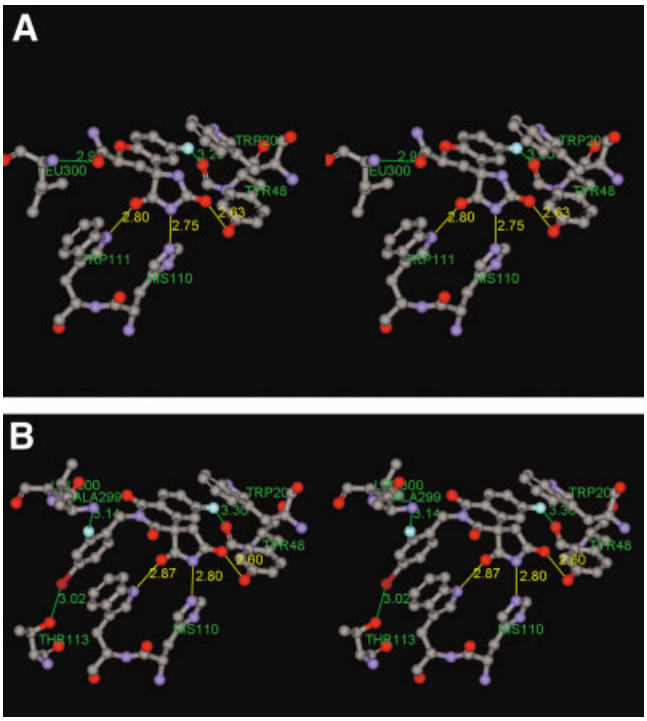

Fig. 5. Stereoviews of (**a**) Fidarestat and (**b**) Minalrestat bound into the active site of the human ALR2 holoenzyme. Residues within 4 Å of the compounds with hydrogen bonds (yellow solid lines) and close contacts (green solid lines) are shown.

As indicated both by the electron density maps and the site geometry, Minarestat binds only with a water molecule linked to His110, whereas Fidarestat binds either with a water molecule or with a Cl^- ion. This difference could be due to an intrinsic different pKa of the two inhibitors. This finding suggests that cyclic imide inhibitors initially cross the biological membrane as neutral compounds and then lose the proton and bind to the enzyme's active site, with their negative charge contributing to the tight inhibitor binding. This observation is supported by the fact that the translation from *in vitro* to *in vivo* activity for this class of compounds was usually easily achieved.[37,40]

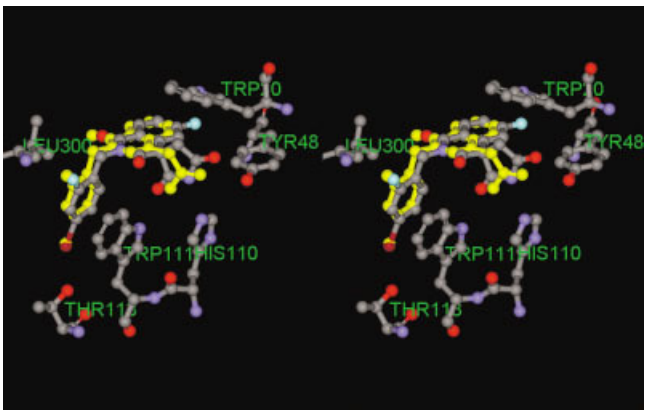

Fig. 7. Stereoview showing the superposition of the active site of human ALR2 with bound Minalrestat (bonds and C = gray, O = red, N = blue, F = cyan, and Br = brown) and Ponalrestat (bonds and C = yellow, O = red, N = blue, F = cyan, and Br = pink).

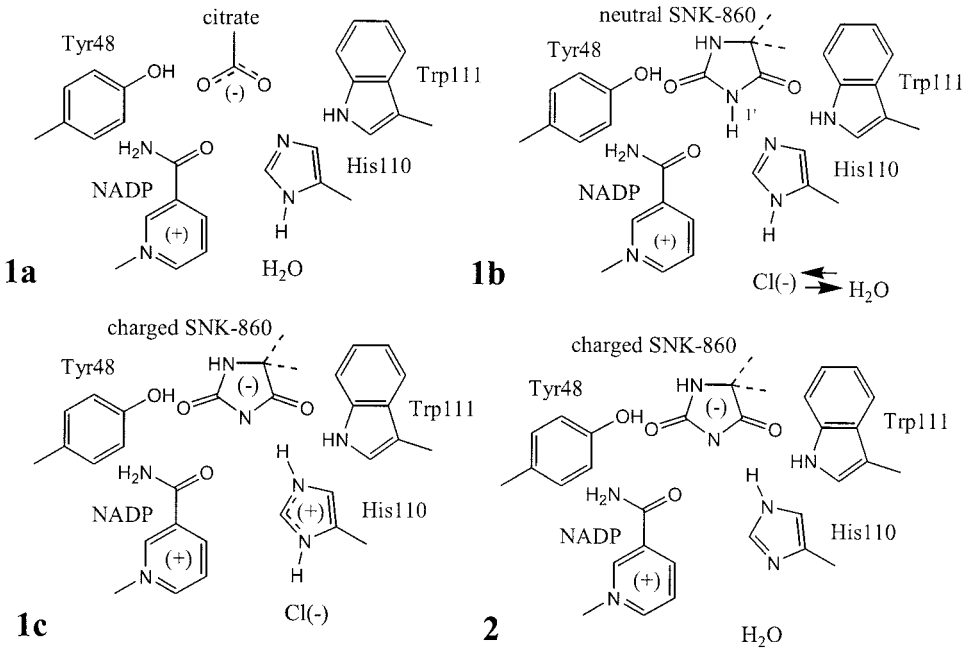

Fig. 6. Proposed mechanism of binding of Fidarestat (SNK-860). Figures were prepared by using PYMOL,[46] ViewerLite(Accelrys) and Molscript.[47]

The orientation of the bound Fidarestat in the active site of human ALR2 holoenzyme is in agreement with an earlier crystallographic investigation conducted at 2.8 Å resolution.[18] In this study, crystals of the ternary complex were grown from buffered ammonium sulfate solutions at pH 7.5 and belonged to the monoclinic space group *C2*. The chroman ring of Fidarestat was located within van der Waals contacts with the side-chains of Trp20, Trp111, Phe122, and Trp219. The oxygen of the carbonyl group was hydrogen-bonded to the main-chain nitrogen atom of Leu300 (Leu300 adopts a double conformation in the atomic resolution structure with hydrogen bond distances equal to 2.96 Å and 3.03 Å). This interaction was suggested to be responsible for the high affinity and selectivity of Fidarestat for ALR2 over ALR1.[18] In Minalrestat binding, the isoquinoline ring system is located in a hydrophobic pocket formed mainly by the side-chains of the following ALR2 residues: Trp20, Phe122, and Trp219 (Fig. 5). The 4-bromo-2-fluorobenzyl group penetrated the crevice formed between Phe122, Leu300, and Trp111. The benzyl group π-stacks against the side-chain of Trp111 (3.65 Å), whereas the bromine atom is positioned within interacting distance with the OG1 atom of Thr113 (3.02 Å) and the fluorine atom is hydrogen bonded to the main-chain amide of Leu300 (3.20 Å).

The binding of the hydrophobic ring systems in Minalrestat and Ponalrestat,[41] a carboxylic acid ARI that had no obvious beneficial effects in clinical trials,[42] are similar (Fig. 7). The polar head groups of the inhibitors interacted with the three active site residues (Tyr48, His110, and Trp111), adding further evidence for a generalized mode of ARI binding. The isoquinoline and phthalazinyl ring systems of Minalrestat and Ponalrestat, respectively, formed similar van der Waals contacts with the enzyme's hydrophobic pocket (Trp20, Phe122, and Trp219) and the 4-bromo-2-fluorobenzyl groups penetrated the specificity pocket, forming similar interactions with Trp111, Thr113, and Leu300. The similarities in the binding modes for the cyclic imide and carboxylic acid inhibitors Minalrestat and Ponarlestat, respectively, suggest that the orientations of the cyclic imide and carboxylic acid inhibitors in the active site of ALR2 are dictated by both the hydrophobic ring system and the polar head group of the inhibitors.

The binding of Minalrestat and Ponalrestat[41] to ALR2 is accompanied by a conformational change to the side-chains of Leu300 and Phe122 that opens the specificity pocket lined by residues Trp111, Thr113, Phe122, Ala299, and Leu300. The 4-bromo-2-fluorobenzyl group of the inhibitors form hydrophobic interactions with ALR2 as well as polar interactions with the side-chain of Thr113 and the main-chain N atom of Leu300. Subatomic resolution studies conducted at IGBMC suggested that the inclusion of a Br atom in the inhibitor's benzyl group improved both affinity and selectivity of ARIs for ALR2 over ALR1 (Howard et al., submitted for publication), because Thr113 in ALR2 is replaced by a Tyr residue in ALR1,[43] which would likely lead to a collision with the Br atom. However, in Fidarestat, an ARI that is 1300 times more potent inhibitor of ALR2 than ALR1,[18] the binding of the inhibitor to ALR2 is not accompanied by a conformational change, because the carbamoyl group of Fidarestat forms a hydrogen bond with the main-chain N atom of Leu300, a residue that lines part of the specificity pocket. This residue is a Pro in ALR1 and its inability to form a hydrogen bond with the inhibitor was attributed to the much higher selectivity of Fidarestat for ALR2.

CONCLUSION

This study provided an understanding of the electrostatic interactions between the cyclic imide substituents of the inhibitors and the holoenzyme. The presence of a Cl^- ion and the difference maps strongly suggest that the protonation of catalytic residue His110 changes during inhibitor binding, from singly protonation at the imidazolium Nδ2 atom position to double protonation and that it forms a hydrogen bond and a strong electrostatic interaction with the negatively charged 1′-position nitrogen atom in the cyclic imide substituents of the inhibitors. The negatively charged head group of the inhibitors also interacted with the positively charged $NADP^+$, adding to the charge complementarity between the holoenzyme and inhibitor. The structures described here show the importance of charge compensation in the active site and the possibility of changing the protonation states. The relevance of these results to the inhibitor activity in vivo is currently being studied. The structures of the ALR2 holoenzyme complexed with Fidarestat and Minalrestat also support previous studies pointing that the ARI interactions with residues from the enzyme's so-called specificity pocket are responsible for selectivity of ALR2 over ALR1. A comparison between the binding sites of Minalrestat and Ponalrestat indicated that the halogenated benzyl ring of the inhibitors met the requirements of steric bulk and chemical properties to enter the specificity pocket of ALR2, resulting in conformational changes to the holoenzyme. On the other hand, the interaction of Fidarestat with the specificity pocket did not induce a conformational change to the holoenzyme, asserting the important role of the specificity pocket in the design of specific inhibitors of ALR2.

Coordinates and structure factors have been deposited in the Protein Data Bank. Access codes are 1PWL for Minalrestat and 1PWM for Fidarestat.

ACKNOWLEDGMENTS

We thank the staff of the SLS and of the SBC, especially Ruslan Sanishvili, for their help in data collection, the IGBMC staff for support with purification, crystallization, and computing facilities, and Eduardo Howard and Alexandra Cousido for fruitful discussions on the crystallization of human ALR2.

REFERENCES

1. Jez JM, Bennett MJ, Schlegel BP, Lewis M, Penning TM. Comparative anatomy of the aldo-keto reductase superfamily. Biochem J 1997;326:625–636.
2. Warren JC, Murdock GL, Ma Y, Goodman SR, Zimmer WE. Molecular cloning of testicular 20 alpha-hydroxysteroid dehydrogenase: identity with aldose reductase. Biochemistry 1993;32:1401–1406.

3. Kinoshita JH, Nishimura C. The involvement of aldose reductase in diabetic complications. Diabetes Metab Rev 1988;4:323–337.
4. Dunlop M. Aldose reductase and the role of the polyol pathway in diabetic nephropathy. Kidney Int Suppl 2000;77:S3–S12.
5. Yabe-Nishimura C. Aldose reductase in glucose toxicity: a potential target for the prevention of diabetic complications. Pharmacol Rev 1998;50:21–33.
6. Oates PJ, Mylari BL. Aldose reductase inhibitors: therapeutic implications for diabetic complications. Exp Opin Invest Drugs 1999;8:1–25.
7. Pfeifer MA, Schumer MP, Gelber DA. Aldose reductase inhibitors: the end of an era or the need for different trial design. Diabetes 1997;46:S82–S89.
8. Costantino L, Rastelli G, Gamberini MC, Barlocco D. Pharmacological approaches to the treatment of diabetic complications. Exp Opin Ther Patents 2000;10:1245–1262.
9. Malamas MS, Hohman TC, Millen. Novel spirosuccinimide aldose reductase inhibitors derived from isoquinoline-1,3-diones:2[(4-bromo-2-fluorophenyl)methyl]-6-fluorospiro [isoquinoline-4(1*H*),3′-pyrrolidine]-1,2′,3,5′(2*H*)-tetrone and congeners. J Med Chem 1994;37:2043–2058.
10. Malamas MS, Hohman TC. N-substituted spirosuccinimide, spiropyridazine, spiroazetidine and acetic acid aldose reductase inhibitors derived from isoquinoline-1, 3-diones. J Med Chem 1994;37: 2059–2070.
11. Negoro T, Murata M, Ueda S, Fujitani B, Ono Y, Kuromiya A, Komiya M, Suzuki K, Matsumoto J. Novel, highly potent aldose reductase inhibitors: R-(-)-2-(4-bromo-2-fluorobenzyl)-1,2,3,4-tetrahydropyrrolo[1,2-a]pyrazine-4-spiro-3′-pyrolidine-1,2′,3,5-tetrone (AS-3201) and its congeners. J Med Chem 1998;41:4118–4129.
12. Kato N, Mizuno K, Makino M, Suzuki T, Yahihashi S. Effects of 15-month aldose reductase inhibition with fidarestat on the experimental diabetic neuropathy in rats. Diabetes Res Clin Pract 2000;50:77–85.
13. Hotta N, Toyota T, Matsuoka K, Shigeta Y, Kikkawa R, Kaneko T, Takahashi A, Sugimura K, Koike Y, Ishii J, Sakamoto N. Clinical efficacy of fidarestat, a novel aldose reductase inhibitor, for diabetic peripheral neuropathy. Diabetes Care 2001;24:1776–1782.
14. Wilson DK, Tarle I, Petrash JM, Quiocho FA. Refined 1.8 Å structure of human aldose reductase complexed with the potent inhibitor zopolrestat. Proc Natl Acad Sci USA 1993;90:9847–9851.
15. Urzhumtsev A, Tête-Favier F, Mitschler A, Barbanton J, Barth P, Urzhumtseva L, Biellmann J-F, Podjarny AD, Moras DA. "Specificity" pocket inferred from the crystal structures of the complexes of aldose reductase with the pharmaceutically important inhibitors tolrestat and sorbinil. Structure 1997;5:601–612.
16. Harrison DHT, Bohren KM, Petsko GA, Ringe D, Gabbay KH. The alrestatin double-decker: binding of two inhibitor molecules to human aldose reductase reveals a new specificity determinant. Biochemistry 1997;36:16134–16140.
17. Rogniaux H, Van Dorsselaer A, Barth P, Biellmann J-F, Barbanton J, Van Zandt M, Chevrier B, Howard E, Mitschler A, Potier N, Urzhumtseva L, Moras D, Podjarny A. Binding of aldose reductase inhibitors: correlation of crystallographic and mass spectrometric studies. J Am Soc Mass Spectrom 1999;10:635–647.
18. Oka M, Matsumoto Y, Sugiyama S, Tsuruta N, Matsushima M. A potent aldose reductase inhibitor, (2*S*,4*S*)-6-Fluoro-2′,5′-dioxyspiro[chroman-4,4′-imidazoline]-2-carboxamide (Fidarestat): its absolute configuration and interaction with aldose reductase by X-ray crystallography. J Med Chem 2000;43:2479–2483.
19. El-Kabbani O, Carper DA, McGowan MH, Devedjiev Y, Rees-Milton KJ, Flynn TG. Studies on the inhibitor-binding site of porcine aldehyde reductase: crystal structure of the holoenzyme-inhibitor ternary complex. Proteins 1997;29:186–192.
20. Barski OA, Gabbay KH, Bohren KM. The C-terminal loop of aldehyde reductase determines the substrate and inhibitor specificity. Biochemistry 1996;35:14276–14280.
21. Lee YS, Chen Z, Kador PF. Molecular modeling studies of the binding modes of aldose reductase inbibitors at the active site of human aldose reductase. Bioorg Med Chem 1998;6:1811–1819.
22. Hohman TC, El-Kabbani O, Malamas MS, Lai K, Putilina T, McGowan MH, Wane Y-Q, Carper DA. Probing the inhibitor-binding site of aldose reductase with site-directed mutagenesis. Eur J Biochem 1998;256:310–316
23. El-Kabbani O, Carper DA, McGowan MH, Ginell SL. Crystal structure of porcine aldehyde reductase at 2.0 Å resolution: modeling an inhibitor in the active site of the enzyme. Protein Pept Lett 1996;3:427–434.
24. El-Kabbani O, Rogniaux H, Barth P, Chung R, Fletcher E, Dorsselaer A, Podjarny A. Aldose and aldehyde reductases: correlation of molecular modeling and mass spectrometric studies on the binding of inhibitors to the active site. Proteins 2000;41:407–414.
25. Chung S, La Mendola J. Cloning and sequence determination of human placental aldose reductase gene. J Biol Chem 1989;264: 14775–14777.
26. Lamour V, Barth P, Rogniaux H, Poterszman A, Howard E, Mitschler A, Van Dorsselaer A, Podjarny A, Moras D. Production of crystals of human aldose reductase with very high resolution diffraction. Acta Crystallogr 1999;D55:721–723.
27. Matthews BW. Solvent content of protein crystals. J Mol Biol 1968;33:491–497.
28. Otwinowski Z, Minor W. Processing of X-ray diffraction data collected in oscillation mode. Methods Enzymol 1997;276:307–326.
29. Calderone V, Chevrier B, Van Zandt M, Lamour V, Howard E, Poterszman A, Barth P, Mitschler A, Lu J, Dvornik DM, Klebe G, Kraemer O, Moorman AR, Moras D, Podjarny A. The structure of aldose reductase bound to the inhibitor IDD384. Acta Crystallogr 2000;D56:536–540.
30. Brünger AT, Krukowski A, Erickson JW. Slow-cooling protocols for crystallographic refinement by simulated annealing. Acta Crystallogr A 1990;46:585–593.
31. Sheldrick G, Schneider T. SHELXL: high-resolution refinement. Methods Enzymol 1997;277:319–343.
32. Roussel A, Cambillau C. TURBO-FRODO molecular graphics program. In: Silicon Graphics Geometry Partner Directory. Mountain View, CA: Silicon Graphics; 1989. p 77–78.
33. McRee DE. XtalView/Xfit—a versatile program for manipulating atomic coordinates and electron density. J Struct Biol 1999;125: 156–165.
34. Laskowski RA, MacArthur MW, Moss DS, Thornton JM. PROCHECK: a program to check the stereochemical quality of protein structures. J Appl Crystallogr 1993;26:283–291.
35. Ramachandran GN, Sasisekharan V. Conformation of proteins and polypeptides. Adv Protein Chem 1968;23:283–437.
36. Rondeau J-M, Tête-Favier F, Podjarny A, Reymann J-M, Barth P, Biellmann J-F, Moras D. Novel NADPH-binding domain revealed by the crystal structure of aldose reductase. Nature 1992;355:469–472.
37. Eggler JF, Larson ER, Lipinski CA, Mylari BL, Urban FJ. A prospective of aldose reductase inhibitors. Adv Med Chem 1993;2: 197–246.
38. Grimshaw CE, Bohren KM, Lai CJ, Gabbay KH. Human aldose reductase: pK of tyrosine 48 reveals the preferred ionization state for catalysis and inhibition. Biochemistry 1995;34:14374–14384.
39. Ehrig T, Bohren KM, Prendergast FG, Gabbay KH. Mechanism of aldose reductase inhibition: binding of $NADP^+$/NADPH and alrestatin like inhibitors. Biochemistry 1994;33:7157–7165.
40. Ashizawa N, Aotsuka T. Benzothiazole aldose reductase inhibitors. Drugs Fut 1998;23:521–529.
41. El-Kabbani O, Ramsland P, Darmanin C, Chung RP-T, Podjarny A. Structure of human aldose reductase holoenzyme in complex with statil: an approach to structure-based inhibitor design of the enzyme. Proteins 2003;50:230–238.
42. Krentz AJ, Honigsberger L, Ellis SH, Hardman M, Nattrass M. A 12-month randomized controlled study of aldose reductase inhibitor ponalrestat in patients with chronic symptomatic diabetic neuropathy. Diabetic Med 1992;9:463–468.
43. El-Kabbani O, Judge K, Ginell SL, Myles DA, DeLucas LJ, Flynn TG. Structure of porcine aldehyde reductase holoenzyme. Nat Struct Biol 1995;2:687–692.
44. Luzzati PV. Traitement statistique des erreurs dans la determination des structures cristallines. Acta Crystallogr 1952;5:802–810.
45. Franken SM, Rozeboom HJ, Kalk KH, Dijkstra BW. Crystal structure of Haloalkane Dehalogenase: enzyme to detoxify halogenated alkanes. EMBO J 1991;10:1297–1302.
46. DeLano WL. PYMOL: an open-source molecular graphics tool. CCP4 Newslett Protein Crystallogr 2002;40:11.
47. Kraulis J : MOLSCRIPT: a program to produce both detailed and schematic plots of protein structures. J Appl Crystallogr 1991;24: 946–950.